Molecular Biology of the Cell
Vol. 15, 2580–2592, June 2004

Markers for Detergent-resistant Lipid Rafts Occupy Distinct and Dynamic Domains in Native Membranes

Bridget S. Wilson,*† Stanly L. Steinberg,‡ Karin Liederman,‡ Janet R. Pfeiffer,* Zurab Surviladze,* Jun Zhang,§ Lawrence E. Samelson,‖ Li-hong Yang,‖ Paul G. Kotula,¶ and Janet M. Oliver*

*Departments of Pathology and Cancer Research and Treatment Center, ‡Mathematics and Statistics, and §Computer Science, University of New Mexico, Albuquerque, New Mexico 87131; ‖Laboratory of Cellular and Molecular Biology, Center for Cancer Research, National Cancer Institute, Bethesda, Maryland 20892; and ¶Materials Characterization Department, Sandia National Laboratories, Albuquerque, New Mexico 87185

Submitted August 8, 2003; Revised December 29, 2003; Accepted February 25, 2004
Monitoring Editor: Jennifer Lippincott-Schwartz

Lipid rafts isolated by detergent extraction and sucrose gradient fractionation from mast cells are enriched for the glycosylphosphatidylinositol-linked protein Thy-1, the ganglioside GM1, palmitoylated LAT, and cross-linked IgE receptors, FcεRI. This study addresses the relationship of fractionation data to the organization of raft markers in native membranes. Immunogold labeling and electron microscopy shows there is little or no colocalization of the raft markers Thy-1, GM1, and LAT with each other or with FcεRI on native membrane sheets prepared from unstimulated cells. External cross-linking of Thy-1 promotes coclustering of Thy-1 with LAT, but not with GM1. Thy-1 and LAT clusters occur on membrane regions without distinctive features. In contrast, external cross-linking of FcεRI and GM1 causes their redistribution to electron-dense membrane patches independently of each other and of Thy-1. The distinctive patches that accumulate cross-linked FcεRI and GM1 also accumulate osmium, a stain for unsaturated lipids, and are sites for coated vesicle budding. Electron microscopy reveals a more complex and dynamic topographical organization of membrane microdomains than is predicted by biochemical analysis of detergent-resistant membranes.

INTRODUCTION

Ordered regions of membrane, known as microdomains, lipid rafts, detergent-resistant membranes (DRMs), and other abbreviations are thought to be critical sites of signal propagation and membrane trafficking (Edidin, 1997, 2001; Simons and Ikonen, 1997; Anderson, 1998; Brown and London, 1998, 2000; Jacobson and Dietrich, 1999; Langlet *et al.*, 2000; Anderson and Jacobson, 2002). Analysis of these regions typically begins with detergent solubilization of whole cells followed by sucrose density gradient centrifugation and the recovery of detergent-resistant membranes from the light fractions of the gradient. The DRMs are enriched for caveolin, glycosylphosphatidylinositol-linked (GPI-linked) proteins, glycosphingolipids, GM1 ganglioside, and cholesterol, suggesting that these components are associated in the liquid-ordered (l_o) phase of the lipid bilayer (Schroeder *et al.*, 1994; Ahmed *et al.*, 1997). The interpretation of gradient centrifugation experiments remains controversial. There is evidence that detergents may force associations between components that are not colocalized in intact cells (Mayor and Maxfield, 1995), and fractionation results are known to be dramatically altered by varying the concentration of Triton X-100 (Field *et al.*, 1999; Parolini *et al.*, 1999), by use of alternative detergents (Montixi *et al.*, 1998; Surviladze *et al.*, 1998) or by omission of detergent altogether (Ilangumaran *et al.*, 1999; Harder and Kuhn, 2000; Surviladze et al., 2001). Methods to observe membrane segregation in situ have also generated controversy. Results based on light and fluorescence microscopy of proteins and lipids, including refinements of the established fluorescence recovery after photobleaching methods and new single particle tracking methods, have led some investigators to conclude that lipid rafts comprise a minor fraction of the cell surface and others to postulate that >50% of the plasma membrane consists of lipid rafts (Kenworthy *et al.*, 2000; Edidin, 2001). Although biochemical analyses imply a rather unitary and stable composition for lipid rafts (Brown and London, 1998), evidence from biophysical and fluorescence imaging studies raises the possibility that raft fractions may be made up of a collection of separate membrane domains with a common ability to resist detergent solubilization (Edidin, 2001; Anderson and Jacobson, 2002; Bunnell *et al.*, 2002).

We have provided new evidence for microdomain organization of plasma membrane components based upon high-resolution electron microscopy and immunogold labeling of native membrane sheets (Wilson *et al.*, 2000, 2001). Our model system is a rat mast cell tumor line, the RBL-2H3 cell, that is rich in surface expression of the high-affinity IgE receptor, FcεRI (>200,000 receptors/cell). Previous work revealed the dynamic redistribution of FcεRI and a subset of signaling molecules during propagation of the FcεRI signal-

Article published online ahead of print. Mol. Biol. Cell 10.1091/mbc.E03–08–0574. Article and publication date are available at www.molbiolcell.org/cgi/doi/10.1091/mbc.E03–08–0574.

† Corresponding author. E-mail address: bwilson@salud.unm.edu.

Abbreviations used: DNP-BSA, dinitrophenol-conjugated bovine serum albumin; FcεRI, the high-affinity receptor for IgE; LAT, linker for activation of T cells; RBL-2H3, rat basophilic leukemia cell line 2H3.

ing cascade. In resting cells, FcεRI is loosely colocalized with acylated Lyn in small clusters. FcεRI cross-linking results in the progressive separation of receptor from Lyn and its redistribution to membrane regions that are characteristically more electron dense than bulk membrane and are often bordered by coated pits. Syk, the kinase linking FcεRI cross-linking to most downstream responses, is rapidly recruited to these patches, and mixes extensively with receptors. A large number of other signaling proteins (Gab2, Vav, Grb2, phospholipase Cγ2 [PLCγ2], phosphatidylinositol 3-kinase, and others) are recruited to these patches, leading to the hypothesis that these areas represent primary sites of active signaling (Wilson *et al.*, 2000, 2001, 2002). We also mapped the distribution of the dually palmitoylated transmembrane adaptor molecule LAT that is critical for FcεRI signaling (Saitoh *et al.*, 2000). LAT is inherently clustered in membranes from resting cells and the small LAT clusters typically coalesce into larger structures within minutes of FcεRI cross-linking. Tightly packed clusters of LAT in activated cells are broadly dispersed, mix poorly with FcεRI aggregates, and may represent secondary signaling sites (Wilson *et al.*, 2001).

Here, we extend the membrane sheet approach to provide insight into the distribution of FcεRI and LAT relative to other "raft" markers that can be recovered within the low-density, detergent-resistant membrane fractions of sucrose density gradients. We focus on comparison with GPI-anchored Thy-1 and GM1 ganglioside that are both enriched in the raft fractions. Cell fractionation confirms the preferential association of these markers with detergent-resistant membranes. Electron microscopy reveals very little colocalization of these raft constituents in native membranes from resting cells. Aggregation of individual raft components such as Thy-1 can promote coclustering with certain raft markers (LAT) and not with others (GM1 and cross-linked FcεRI). We identify the electron-dense regions of membranes as sites of osmium accumulation, consistent with enrichment in unsaturated fatty acids. These regions are also sites of internalization for aggregated FcεRI and aggregated GM1. High-resolution electron microscopy reveals a more complex and challenging topographical organization of membrane microdomains than is predicted from fractionation studies.

MATERIALS AND METHODS

Antibodies and Gold Reagents

Monoclonal antibodies to the FcεRI β subunit were kindly provided by Dr. Juan Rivera (National Institutes of Health, Bethesda, MD). Monoclonal anti-Thy1 antibodies (OX7) were purchased from BD Biosciences (Palo Alto, CA), monoclonal anti-CD4 (H-370) antibodies were from Santa Cruz Biotechnology (Santa Cruz, CA), and rabbit polyclonal anti-LAT antibodies were from Upstate Biotechnology. Biotinylated cholera toxin was from Sigma-Aldrich (St. Louis, MO). Gold-conjugated anti-mouse and anti-rabbit secondary antibodies and gold-conjugated streptavidin were from Amersham Biosciences (Piscataway, NJ).

RBL-2H3 Stimulation

Cells were plated on 15-mm-round, clean glass coverslips and primed with IgE (1 μg/ml) overnight. After washing, FcεRI was cross-linked by incubation with dinitrophenol-conjugated bovine serum albumin (DNP-BSA) (0.1–1 μg/ml) or with gold conjugated-DNP-BSA. To aggregate Thy-1, cells were incubated for 10 min at room temperature (RT) with anti-Thy1 (1 μg/ml), followed by cross-linking at 37°C with gold-conjugated anti-mouse antibodies (diluted from manufacturer's stock, 1:5). To aggregate GM1 ganglioside, cells were incubated for 10 min at RT with biotinylated cholera toxin (20 μg/ml) and cross-linked for indicated times at 37°C with avidin-gold.

For stable transfection, green fluorescent protein (GFP)-LAT and CD4-LAT constructs were engineered into the pcDL-SRα296 expression vector (Wilson *et al.*, 1995). Cells expressing CD4-tagged LAT were initially enriched by positive selection by using magnetic beads coated with anti-CD4 antibodies (source). Approximately 2 wk later, cells were labeled with fluorescent anti-CD4 antibodies and those cells with high surface expression selected by fluorescence activated cell sorting. Stable transfectants expressing GFP-LAT were also sorted by fluorescence activated cell sorting.

Isolation and Analysis of Detergent-resistant Lipid Rafts

IgE-primed RBL-2H3 cells (40×10^6) were harvested from suspension culture dishes with 1.5 mM EDTA in Hanks' buffered saline without divalent cations. Washed cells were resuspended in Hanks' buffered saline, divided into two aliquots, and held for 2 min at 37°C with or without DNP-BSA (1 μg/ml). Cells were collected by centrifugation at 4°C, cell pellets were resuspended in 750 μl of ice-cold lysis buffer (10 mM Tris-HCl, pH 8.0, 0.05% Triton X-100, 50 mM NaCl, 10 mM EDTA, 10 mM glycerophosphate, 1 mM $NaVO_4$, and 1× protease inhibitor cocktail from Roche Diagnostics, Indianapolis, IN). Lysates were mixed with 750 μl of 80% sucrose (prepared in 10 mM Tris-HCl, pH 8.5, 50 mM NaCl, and 2 mM EDTA) and overlaid onto 0.5 ml of 80% sucrose in polyallomer tubes (13 × 51 mm), followed by 0.5-ml layers of 35, 25, and 20% and 0.6-ml aliquots of 15 and 10%. The gradient was centrifuged in a SW 55 (Beckman Coulter, Fullerton, CA) rotor at 200,000 × *g* for 16 h at 4°C. Fractions (0.5 ml) were harvested sequentially from the top of the gradient. For analyses of protein composition, aliquots (35 μl) were mixed with equal volume of 2× SDS sample buffer, boiled for 5 min, and separated by 8 or 10% SDS-PAGE. Proteins were transferred to nitrocellulose by using a semidry blotting system (Labconco, Kansas City, MO). Blots were probed with primary antibodies (1 μg/ml) followed by horseradish peroxidase (HRP)-conjugated secondary antibodies (antimouse HRP-conjugates were diluted 1:10,000 and anti-rabbit HRP-conjugates were diluted 1:40,000); immunolabeled proteins were visualized by fluorography (enhanced chemiluminescence; Pierce Chemical, Rockford, IL). To localize GM1, cells were pretreated at room temperature with biotinylated cholera toxin and visualized on blots by using avidin-HRP and fluorography.

Preparation of Plasma Membrane Sheets and Gold Labeling for Transmission Electron Microscopy (TEM) and Scanning Transmission Electron Microscopy (STEM)

To prepare plasma membrane sheets, coverslips were rapidly chilled by immersion in ice-cold HEPES buffer (25 mM HEPES, pH 7, 25 mM KCl, 2.5 mM Mg acetate) and inverted onto nickel electron microscopy grids that had been coated with Formvar and carbon and, on the day of the experiment, glow-discharged and floated on poly-L-lysine (0.8 mg/ml for 30 min, followed by 10 s-distilled H_2O [dH_2O] rinse and air drying). Pressure was applied to the coverslip for 20 s by bearing down with a cork. The coverslips were lifted, leaving sections of the upper cell surface adherent to the poly-L-lysine–coated grid. Membranes were fixed in 2% paraformaldehyde for 10 min at 4°C immediately after cell stimulation and sheet preparation, a process requiring <30 s. For experiments exploring the inherent distribution of GM1 or Thy-1, cells were fixed with paraformaldehyde for 7 min at room temperature and then incubated with gold reagents at room temperature prior to preparation of membrane sheets. FcεRI β subunits were labeled from the inside by incubating sequentially with primary antibodies and gold-conjugated secondary reagents, where grids were inverting onto droplets. Samples were then postfixed in 2% glutaraldehyde in phosphate-buffered saline. Next, samples were stained for 10 min with 1% OsO_4 prepared in 0.1 M cacodylate buffer and washed 5 min with cacodylate buffer and twice for 5 min in dH_2O. Samples were then processed for 10 min in 1% aqueous tannic acid, followed by two 5-min rinses with dH_2O, 10 min with 1% aqueous uranyl acetate, and two 1-min rinses with dH_2O. Grids were air-dried and examined using a Hitachi 600 transmission electron microscope. For x-ray spectral imaging, grids were analyzed using a Phillips FEI Tecnai F30-ST equipped with an EDAX r-TEM SUTW energy dispersive x-ray detector. Spectral images were collected with the Tecnai Imaging and Analysis software at a resolution of 128 × 128 pixels (16,384 spectra) at 1024 channels/spectrum. Details of multivariate statistical analysis methods are provided in Kotula *et al.* (2003).

Mapping Gold Particle Distributions

Electron microscopy negatives were digitized using an ArtixScan1100 scanner (Microtek, Hsinchu, Taiwan). ImageJ was the platform for image analysis. A customized plugin was built to count and find the coordinates of the particles automatically. For 10-nm particles, the plugin uses cropping and thresholding to produce a file of gold particle coordinates; a filtering algorithm is additionally needed to identify 3- and 5-nm particles. Errors (i.e., missed or false particles) are typically <5% and are corrected using an interface provided by the plugin. The ImageJ plugin is also used to identify and quantify cluster size, as well as percentage of coclustering when two sizes of gold are used.

Statistical Analysis

For a statistical measure of clustering, coordinates of gold particles were analyzed using the Hopkins spatial statistic (Jain and Dubes, 1988). To define this statistic, let the coordinates of the n gold particles in an image of a TEM micrograph be given by $p_i = (x_i, y_i)$. Let $m \ll n$ and then choose m random sampling points $s_j = (x_j, y_j)$ in the image and also choose m random gold particles $\tilde{P}_k = P_{ik}$. If $s = (x,y)$ is any point in the image and then $d(s)$ is the

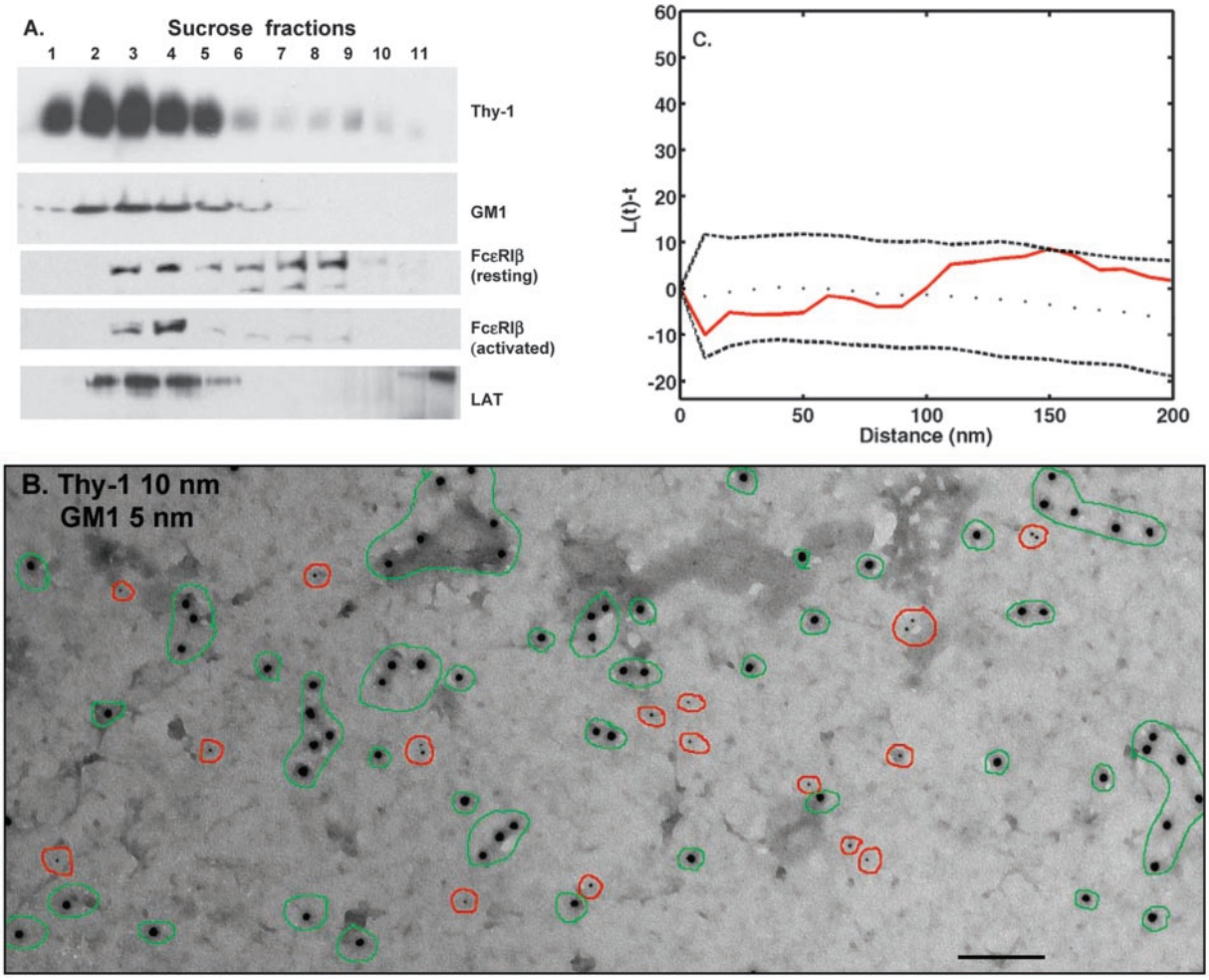

Figure 1. (A) Distributions of raft markers in sucrose density gradients. RBL-2H3 cells were lysed in buffer containing 0.05% Triton X-100, and lysates were overlaid onto discontinuous sucrose gradients. After ultracentrifugation, fractions were analyzed by SDS-PAGE and Western blotting. (B) Distribution of GM1 ganglioside and GPI-anchored Thy-1 in native RBL membranes. Cells were fixed with 2% paraformaldehyde and then Thy-1 and GM1 were labeled from the outside by using anti-Thy-1-gold (10 nm) and biotinyl-cholera toxin-avidin-gold (5 nm). Membrane sheets were prepared, postfixed with glutaraldehyde, and observed by TEM. Green outlines mark clusters of Thy-1 and red circles mark GM1. There is no significant colocalization. Bar, 100 nm. Note that 10-nm gold particles in all figures provide an internal size measurement. (C) Analysis of GM1 and Thy-1 covariance by using Ripley's K statistic. Experimental values for L(t) − t (solid red line) fall within the boundaries predicted for pairwise sets of random points (dashed lines), confirming lack of Thy-1 and GM1 colocalization.

minimum distance to all other gold particles. If $U = \Sigma[low]j - 1d^2(s_j)$ and $W = \Sigma[low]k = 1d^2(\bar{p}_k)$, then the Hopkins statistic is $H = U/(U + W)$. The values H lie in the interval]0,1[. For points generated using a homogeneous Poisson process, the expected value is ½, whereas if the points are clustered the value of H is closer to 1. The probability density function for H is given by

$$f(H) = \frac{H^{m-1}(1-H)^{m-1}}{\Gamma(m)^2\Gamma(2m)}.$$

The Hopkins statistic was used on biological data and on randomly generated patterns of particles in a region of the same size as the micrographs. For the analysis, we choose $m = 5$, and then choose m random sampling points and m unbiased gold particles and compute the value H (see Supplemental Figure 6.) We repeat this for $k = 1000$ times and then form a histogram of these data using b bins. The histogram can be viewed as giving the (piecewise constant) function N(H), $0 \leq H \leq 1$. This histogram is normalized by setting n(h) = b N(H)/k so that it produces a relative frequency distribution that is compared with the theoretical density function $f(H)$. The calculation was performed using a Matlab tool kit developed for the analysis of gold particle data.

Ripley's K function was used to define spatial relationships of two different sizes of gold. Let L(t) − t for each distance t, where L(t) = (K(t)/π)1/2, and K(t) is the Ripley's K function. For a single size of gold particles where distribution is consistent with a homogenous Poisson process, L(t) − t is equal to 0 for all t. Bivariate distribution patterns are analyzed using the SPPA program of Haase (1995) that incorporates the cross-type Ripley's K function (http://home.t-online.de/home/haasep/). Experimental values for L(t) − t are plotted against t for each 20-nm interval up to 200 nm. These are plotted relative to reference values for L(t) under complete spatial randomness (CSR), with a 99% confidence envelope for CSR estimated from 100 Monte Carlo simulations. When experimental values fall outside the confidence envelope, the deviation from CSR is statistically significant.

RESULTS

Recovery of Membrane Components in Light-density Fractions

Figure 1 documents the biochemical properties of all of the membrane constituents mapped at high resolution in this study, based upon flotation of detergent-solubilized proteins within a sucrose density gradient. These constituents are the high-affinity IgE receptor, identified using antibodies to the FcεRI β subunit; the GPI-anchored protein Thy-1; the

palmitoylated transmembrane adaptor LAT; and the ganglioside GM1, a cell surface receptor for cholera toxin. Of these, Thy-1, LAT, and GM1 are constitutively found in the light fractions of the gradient, consistent with their identification as lipid raft markers. When isolated from resting cells, FcεRI is distributed through both heavy and light fractions of the gradient. After activation, there is a marked shift in FcεRI to the light fractions. Similar results were published previously (Draberova and Draber, 1993; Field *et al.*, 1995, 1997, 1999; Surviladze *et al.*, 2001; Draber and Draberova, 2002), leading to a view of lipid rafts as units with a fundamentally stable complement of lipids and lipid-anchored proteins plus an ability to recruit interacting molecules. The problem we address here is the relationship of fractionation data to the organization of the membrane before detergent extraction and fractionation.

The Raft Marker Thy-1 Is Inherently Clustered and Does Not Mix with GM1

Figure 1B demonstrates the use of membrane sheets to define the inherent distributions of the raft markers Thy-1 and GM1 in the outer leaflet of the membrane bilayer of resting cells. In this experiment, cells were fixed with paraformaldehyde, and then incubated with antibodies specific for Thy-1 (10-nm gold) and biotinylated cholera toxin-avidin gold to mark GM1 (5-nm gold). Thy-1 label is distributed over the whole membrane as singlets and small dispersed clusters that range in size from two to 10 gold particles per cluster (Figure 1B, green circles). GM1 label is also distributed over the whole membrane, primarily as singlets that rarely colocalize with Thy-1 (Figure 1B, red circles). To confirm that Thy-1 and GM1 do not colocalize significantly in resting membranes, we used NIH ImageJ and a customized plugin to map the coordinates of the gold particles. Ten micrographs from two separate experiments were analyzed for percentage of coclustering by using an in-house clustering algorithm; the percentage of coclustering in all cases was $<1\%$. This provides direct proof that the recovery of two raft markers in light-density fractions does not predict their codistribution on native membranes.

Previous work showed the utility of Ripley's K function for gold particle analysis when one or more sizes of gold are used (Wofsy *et al.*, 1995; Philimonenko *et al.*, 2000; Prior *et al.*, 2003). As described in MATERIALS AND METHODS, we modified the cross-type Ripley's K statistic function of Haase (1995) to verify results of visual analysis and of the clustering algorithm. Results are shown in Figure 1C, where the experimental values for $L(t) - t$ (solid line) are plotted relative to reference values (dotted lines) that represent the range of values expected for pairs of different sized particles whose distributions are completely random. Because the pairwise values for Thy-1 and GM1 fall within the dotted lines, the incidence of colocalization is not significant. (Additional examples of the Ripley's K test for covariance are found in Figures 6 and 7).

We applied a second spatial statistic function defined by Hopkins (Jain and Dubes, 1988), to determine whether these two raft markers are clustered in native membranes (Figure 2). Figure 2A illustrates the application of the Hopkins statistic to a computer-generated random pattern of points (left). The corresponding bar chart (right) shows that the frequency of these points are evenly distributed around the value of 0.5, generating a profile that is close to the analytic curve (solid line) expected for a random distribution. The Hopkins statistic is designed so that clustered data move the peak of the relative frequency distribution to the right. Figure 2B applies the Hopkins test to the gold distribution from membrane sheets prepared from fixed cells labeled with anti-Thy-1 gold reagents. The Hopkins value is shifted to the right in Figure 2B, showing that the distribution of Thy-1 is inherently nonrandom. This is in marked contrast to the Hopkins analysis of GM1 distribution on resting cells (Figure 2D), where the frequency distribution is very close to random; a slight shift to the right reflects occasional doublets of gold particles labeling GM1 on resting membranes. Thus, Thy-1is inherently clustered in mast cell membranes, as might be expected for potential residents of liquid-ordered domains. However, GM1, widely considered as a resident of these domains, has an essentially random distribution.

The distributions of Thy-1 and GM1 were also evaluated when either raft marker was cross-linked externally before preparation of sheets (Figure 2, C and E). When gold-conjugated antibodies were added to cross-link Thy-1 at 37°C (10 min) before fixation and generation of membrane sheets, Thy-1 clusters increase in size (Figure 2C, left). This results in a further shift to the right when analyzed by the Hopkins statistic (Figure 2C, right). When biotinylated cholera toxin plus streptavidin-gold was added to live cells at 37°C to aggregate GM1, analysis of the resulting membrane sheets shows coalescence of GM1 into a few large clusters (Figure 2, D and E). As expected, the Hopkins value for aggregated GM1 is strongly shifted to the right and reflects a nonrandom distribution (Figure 2E).

Aggregated GM1 and FcεRI, but Not Thy-1, Concentrate in Electron-dense Membrane Regions and Are Endocytosed through Clathrin-coated Pits

We examined membrane sheets double labeled for Thy1 and GM1 that had been aggregated simultaneously, but by using independent reagents, at 37°C. Thy-1 was cross-linked using monoclonal anti-Thy-1 antibodies and 10-nm anti-mouse gold; GM1 was aggregated with biotinylated cholera toxin and 5-nm streptavidin gold. Results are shown in Figure 3A. The dramatic observation here is that aggregated GM1 (red circles), and not aggregated Thy-1 (green circles), is specifically recruited to electron-dense patches. This reinforces the concept that these two raft markers have distinctive patterns of behavior in native membranes.

Figure 3B provides a magnified view of aggregated GM1 in an electron-dense patch. Gold label for GM1 is seen throughout an elongated patch that contains a flat clathrin array (center); three coated vesicles contain GM1 gold label. These patches seemed remarkably like those shown previously to accumulate cross-linked FcεRI during signaling and internalization of receptors (Wilson *et al.*, 2000, 2001). This result led us to compare the distributions of both Thy-1 and GM1 with FcεRI in membrane sheets. In the experiment shown in Figure 3C, IgE-primed cells were stimulated with DNP-BSA-gold (5 nm) for 5 min to cross-link FcεRI. Cells were then fixed, labeled with anti-Thy-1-gold (10 nm), and sheets were generated. The micrograph shows a large membrane domain containing abundant receptors. The entire patch of membrane concentrating receptors is electron dense; an inset shows the typical appearance of small 5-nm gold particles marking receptors in a coated vesicle budding from an electron-dense patch. Under these conditions, 10-nm gold particles marking Thy-1 are found throughout the membrane preparation. Thus, Thy-1 is not excluded from electron-dense patches that accumulate aggregated receptors, occurring there with similar density as elsewhere on the membranes. Because Thy-1 labeling is observed occasionally in coated pits in both resting and activated membranes (large 10-nm gold particles; Figure 3C, inset), it is also not excluded from the pits. This adds a new dimension to concepts of membrane heterogeneity: whereas other mem-

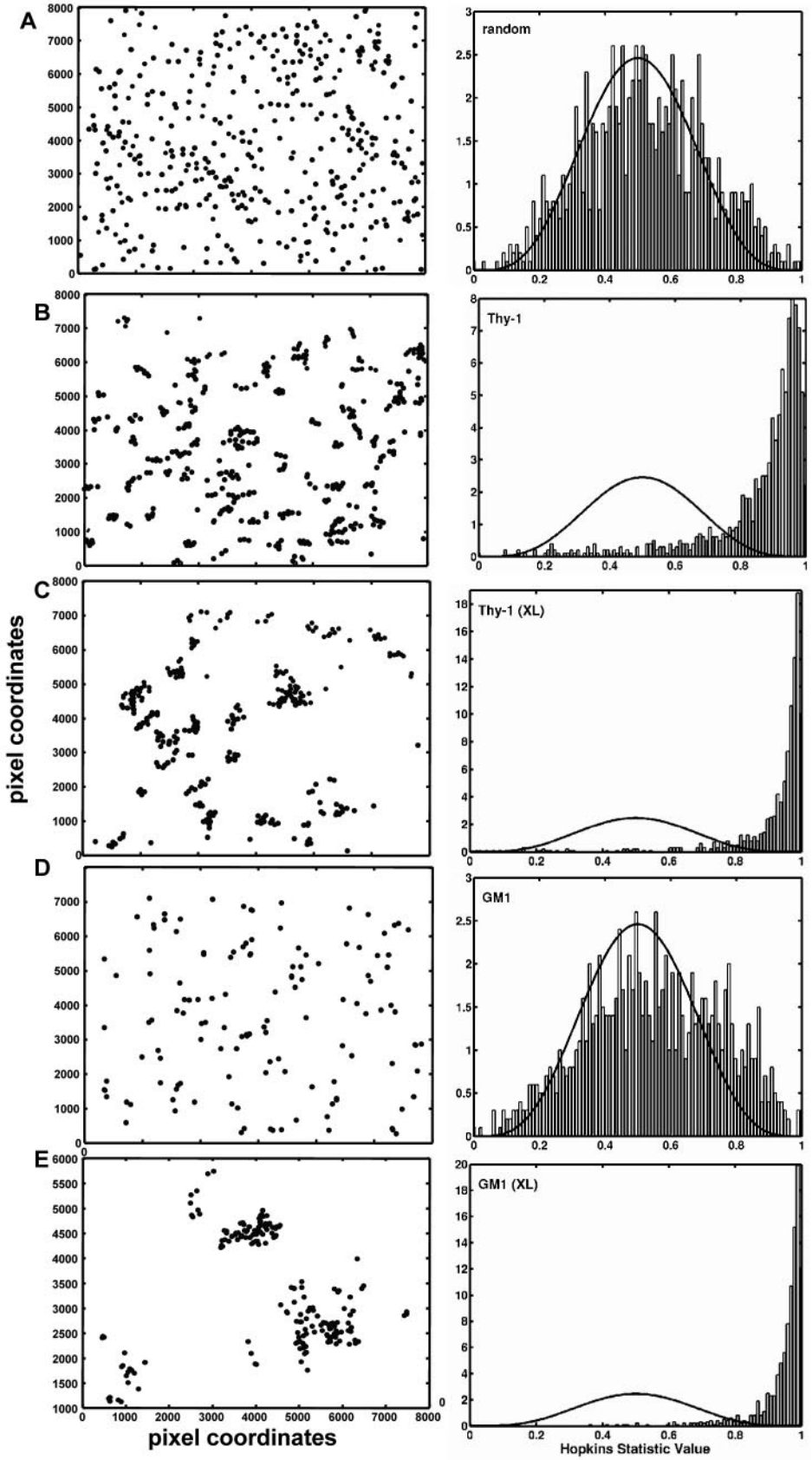

Figure 2. Analysis of clustering using the Hopkins statistic. (A) Pictogram of 300 computer-generated randomized points is shown at left. The corresponding histogram of the relative frequency distribution (at right) shows Hopkins values centered around 0.5, as expected for a random distribution. (B) Experimental sample demonstrating the inherent distribution of Thy-1 on native membrane sheets. The histogram (at right) shows the Hopkins value is shifted to the right, indicating that Thy-1 is significantly clustered. (C). Same as B, except that Thy-1 was aggregated with anti-Thy-1-gold particles for 10 min at 37°C. The histogram shows a further shift to the right, reflecting an increase in clustering. (D) Experimental sample demonstrating the resting distribution of GM1 on native membrane sheets. The histogram shows an essentially random distribution of GM1. (E) Same as in D, except that GM1 ganglioside was aggregated with biotinyl-cholera toxin-avidin-gold for 10 min at 37°C. The histogram shows a high degree of clustering.

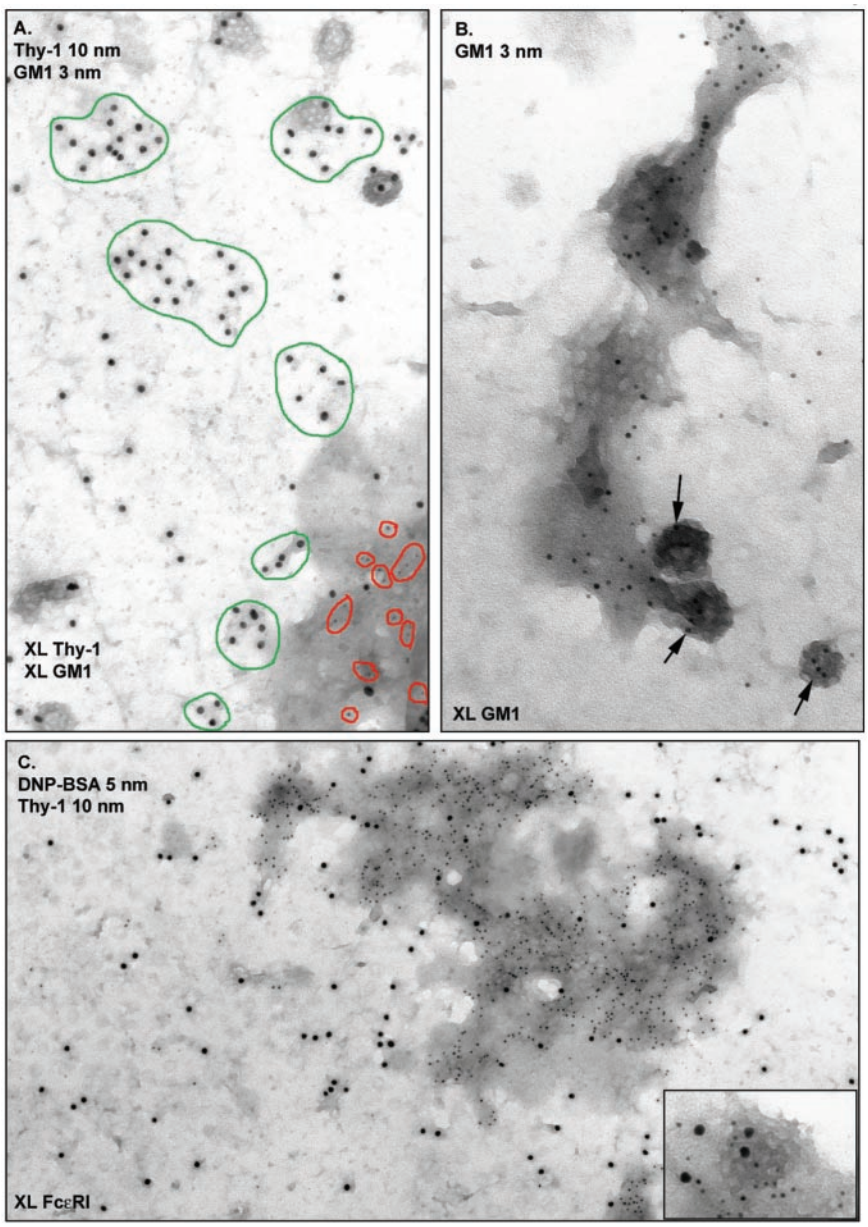

Figure 3. Distributions of Thy-1 and GM1, with and without external cross-linking. (A) Distinct distributions of aggregated Thy-1 and aggregated GM-1. Cells were incubated for 15 min at room temperature with anti-Thy-1 monoclonal antibody and biotinyl-cholera toxin, followed by 10 min at 37°C with 10-nm anti-mouse-gold and 3-nm avidin-gold to aggregate Thy-1 and ganglioside independently and simultaneously. Aggregated GM1 (red outlines) redistribute to electron dense patches (bottom right). In contrast, Thy-1 clusters (green outlines) show no apparent preference for particular membrane regions. (B) Higher magnification view of a GM1-gold aggregate. Gold particles marking GM1 are again seen in a large dark patch. They are additionally seen in the flat clathrin array (middle) and three clathrin-coated vesicles (arrows) budding from the membrane. (C) Distribution of Thy-1 and cross-linked FcεRI. IgE-primed cells were stimulated for 5 min with DNP-BSA-gold (5 nm) and then fixed and labeled with anti-Thy-1-gold (10 nm). Aggregated receptors marked with small gold are concentrated in an electron-dense patch. In contrast, Thy-1 is distributed over the entire membrane. (C, inset) High magnification of coated vesicle from another area on the same sample. Cross-linked FcεRI (small gold) and Thy-1 (large gold) can both enter coated pits.

brane components can be topographically restricted, clusters of Thy-1 can apparently move into and out of specialized membrane features such as electron-dense patches and clathrin-coated pits.

Figure 4, A–C, compares the distributions of FcεRI with GM1 when either one is aggregated alone (Figure 4, A and C) and when they are cross-linked simultaneously at 37°C (Figure 4B). Cross-linked FcεRI (Figure 4A) and GM1 (Figure 4C) are each recruited to electron-dense patches. When both are cross-linked by separate reagents at the same time, they are found in the same patch (Figure 4B). Gold particles marking both receptors and ganglioside are also seen as coated vesicle cargo in these sites (Figure 4B). These results identify the electron-dense patch as a microdomain that is specialized for the dual functions of signal propagation and clathrin-mediated endocytosis. Several points emerge from the GM1 labeling experiments. First, cross-linking FcεRI, but not GM1, causes an increase in patch size and in the abundance of coated vesicles at their periphery. This suggests that patches preexist but become more prominent membrane features during FcεRI signaling. The mechanism is unknown but could involve coalescence of existing patches or membrane lipid remodeling. Additionally, the inherently random distribution of GM1 is inconsistent with previous work using fluorescent cholera toxin as a "raft marker" in two-color comparisons with fluorescent signaling molecules in live cells (Stauffer and Meyer, 1997). Because cholera toxin is pentameric (Reed *et al.*, 1987; Ribi *et al.*, 1988), it is likely that the fluorescent toxin, like the gold-conjugated toxin, induces the redistribution of GM1 from a dispersed topography to signaling domains that independently accumulate activated receptors. We suggest using fluorescent cholera toxin not as a marker for lipid rafts, but rather as a marker for membrane regions that are specialized for signal propagation and endocytosis.

Dark Patches of Membrane Accumulate Osmium, a Stain for Lipids with Double Bonds

We coined the term "osmiophilic patch" because the electron-dense nature of the membrane regions that accumulate

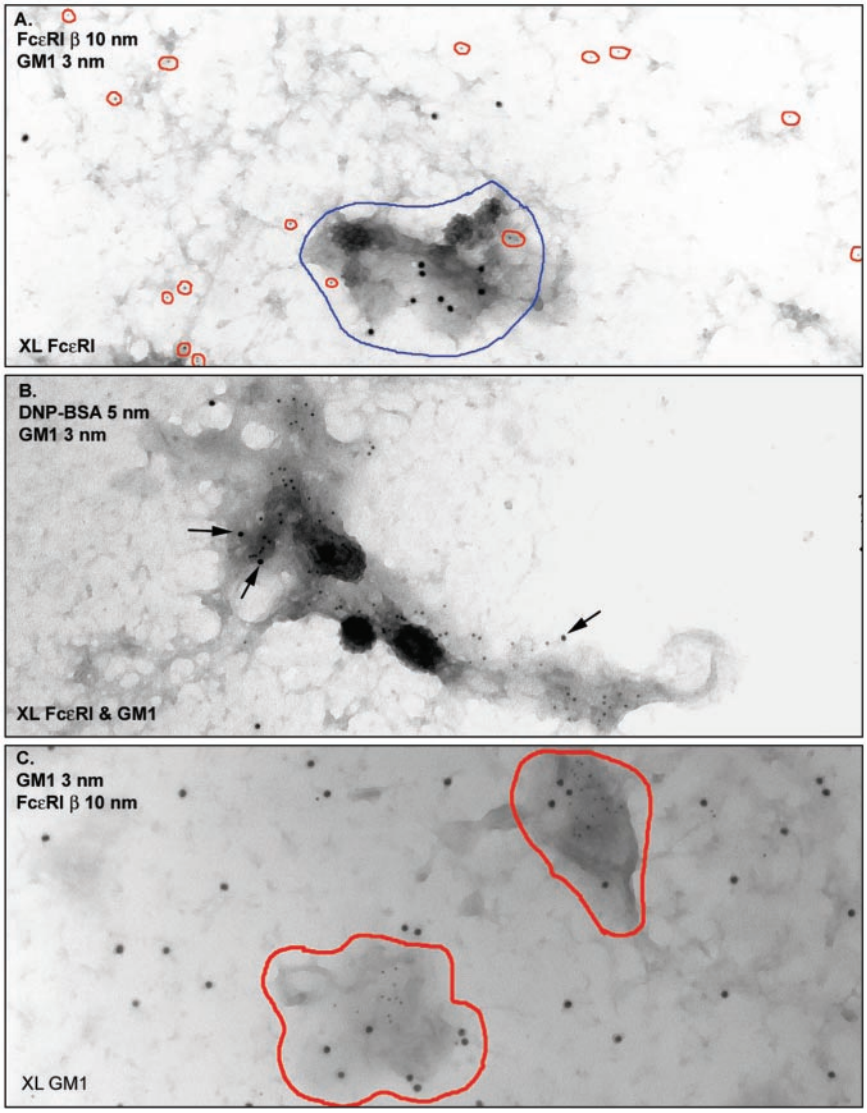

Figure 4. GM1 and FcεRI are independently recruited to dark patches. (A) IgE-primed cells were stimulated for 2 min with DNP-BSA and then fixed and labeled with biotinyl-cholera toxin-avidin-gold (5 nm, outlined in red). Sheets were labeled with anti-FcεRI β-gold (10 nm). The electron-dense patches (outlined in blue) accumulate cross-linked FcεRI but have few particles marking GM1. (B) IgE-primed cells were incubated for 15 min at RT with biotinyl-cholera toxin, followed by 2 min at 37°C with both avidin-gold (5 nm) and DNP-BSA-gold (10 nm). Both cross-linked GM1 (abundant 5-nm gold particles) and cross-linked FcεRI (10-nm particles, arrows) are found within the same dark patch of membrane. Many small gold particles marking GM1 are found within coated vesicles. (C) GM1 was aggregated with biotinyl-cholera toxin-avidin-gold for 10 min at 37°C, membrane sheets were prepared and fixed, and then cells were labeled with antibodies marking FcεRI β. Cross-linked GM1 are exclusively found in dark patches of membrane (outlined in red), in contrast to the labeling for singlets and small clusters of uncross-linked FcεRI that are neither excluded nor concentrated in dark membrane.

cross-linked FcεRI, GM1, and many signaling proteins is markedly reduced in the absence of osmium (Wilson *et al.*, 2000). To validate the nomenclature, we stained membrane sheets with osmium tetroxide but not uranyl acetate and imaged them using a FEI/Philips Electron Optics Tecnai F30-ST, 300-kV TEM/STEM equipped with an energy dispersive x-ray spectrometer, electron energy-loss spectrometer/imaging filter, and Automated eXpert Spectral Image Analysis (AXSIA) software (Kotula *et al.*, 2003). Figure 5A is a STEM bright-field image of a membrane sheet prepared from antigen-stimulated RBL-2H3 cells. The image shows several typical electron-dense patches. Figure 5B is the annular dark-field image of this same area; the two dark patches in Figure 5A show up as light areas in the dark-field STEM image. At bottom is shown the composite spectral analysis of this region, with x-ray peaks corresponding to the grid support composed of nickel, as well as carbon in the sample. Also shown are peaks that correspond to x-ray lines expected for osmium and oxygen bonded to the membrane. Pixel-by-pixel values for carbon (Figure 5C) and osmium (Figure 5D) are depicted for the area shown in Figure 5B, by using a pseudocolor scale. Carbon is enriched in the two large dark patches of membrane, perhaps reflecting the density of signaling molecules and endocytic machinery present in these dark regions. Osmium labeling is also markedly enhanced in the dark patches, suggesting the presence of lipids (or cholesterol) that contain double bonds (March, 1977).

Aggregation of Thy-1 Leads to Increased Coclustering with Palmitoylated LAT

Despite restriction of Thy-1 and other GPI-anchored proteins to the outer leaflet of the plasma membrane, aggregation of this class of molecule can lead to productive intracellular signaling. We explored the possibility that signaling is promoted because aggregated Thy-1 clusters coalesce with clusters of other membrane constituents that are themselves capable of coupling to intracellular machinery. A good candidate is the transmembrane adaptor LAT, whose cytoplasmic tail has both palmitoylation and tyrosine phosphorylation sites and that is inherently clustered in the membranes of RBL cells (Wilson *et al.*, 2001). Figure 6A shows the results of double labeling experiments where cells were prefixed and labeled with mouse anti-Thy-1 gold (10 nm) on the outside before preparing membrane sheets, fol-

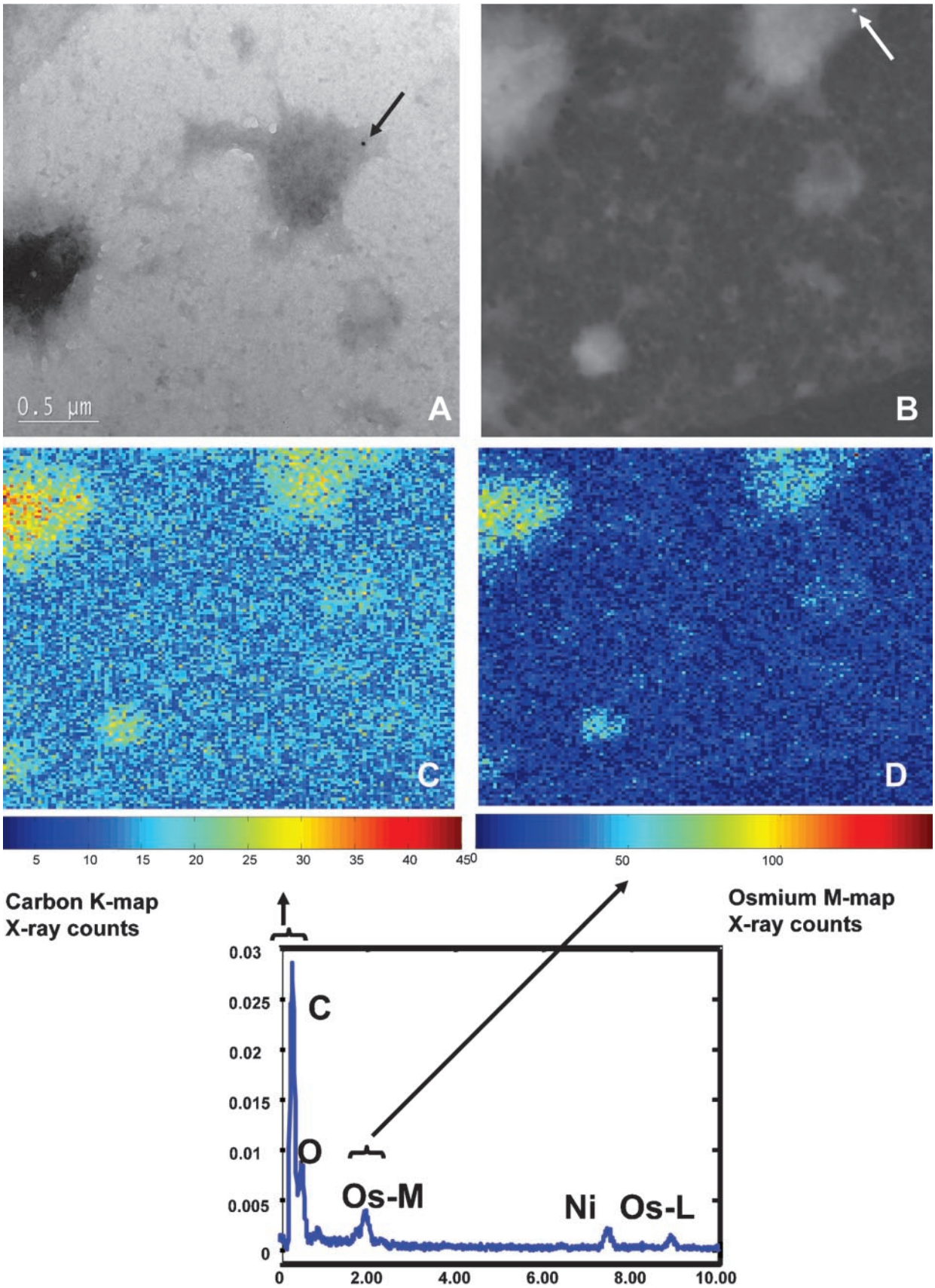
0.5 μm
A
B
C
D
5
10
15
20
25
30
35
40
45
0
50
100
Carbon K-map
X-ray counts
Osmium M-map
X-ray counts
0.03
0.025
0.02
0.015
0.01
0.005
0
C
O
Os-M
Ni
Os-L
0
2.00
4.00
6.00
8.00
10.00

Figure 5.

lowed by labeling of LAT on the cytoplasmic face of sheets by using rabbit anti-LAT-5-nm gold. In these resting membranes, there is observable mixing of Thy-1 and LAT clusters; two mixed clusters are marked with arrows in this micrograph. To quantify this, we mapped the coordinates of the gold particles for ten micrographs from each of two separate experiments and the percentage of coclustering was scored by the clustering algorithm. The extent of Thy-1 clusters that contained LAT ranged from 1 to 23% in these micrographs; analysis using the Ripley's K function (Figure 6D) confirms that the colocalization of Thy-1 and LAT is significant in membranes from resting cells.

Results in membranes from resting cells were compared with those in membranes prepared from cells incubated with anti-Thy-1-gold for 5 or 10 min at 37°C to aggregate Thy-1 (Figure 6, B and C). As Thy-1 aggregate size increases, so does the extent and complexity of mixed LAT and Thy-1 clusters. In a total of seven micrographs (10-min Thy-1 aggregation) used for image analysis, the percentage of Thy-1 clusters that also contained LAT ranged from a low of 21 to a high of 43%. Analysis of covariance using Ripley's K again shows that coclustering of Thy-1 and LAT under these conditions is significant (Figure 6E).

Coclustering of Chimeric CD4-LAT with Endogenous LAT Requires Features in the Cytoplasmic Tail

Unlike GM1, LAT behaves as one might predict for a raft protein: it is inherently clustered in resting membranes; it has two acylation sites that permit incorporation of palmitate, a saturated fatty acid; and it colocalizes with GPI-anchored Thy-1 after Thy-1 aggregation. We expressed a recombinant CD4-LAT chimeric protein in RBL cells to determine whether clustering of LAT is dependent upon features in its transmembrane membrane region or its cytoplasmic tail. The design of the constructs is illustrated in Figure 7A. Endogenous LAT has a very short extracellular domain (four amino acids) and cannot be labeled from the outside of cells by using antibodies. In the recombinant proteins, LAT is extended by the extracellular domain of human CD4 and expressed with either 1) the wild-type LAT transmembrane domain and wild-type LAT cytoplasmic tail (CD4-LAT), or 2) the wild-type LAT transmembrane domain and a truncated cytoplasmic tail that lacks both palmitoylation and phosphorylation sites (CD4-LAT41). Surface expression of CD4 in stable transfectants was confirmed by flow cytometry with commercial antibodies to CD4 (Figure 7B). These cells were fixed, stained from the outside by using monoclonal anti-CD4 gold reagents (10-nm gold), followed by preparation of sheets and staining from the inside by using anti-LAT antibodies (5-nm gold). In the case of CD4-LAT expressing the wild-type cytoplasmic tail, essentially all of the 5-nm clusters (marking both endogenous and chimeric LAT) contain 10-nm gold marking the extracellular CD4 motif (Figure 7C). In the case of the truncated CD4-LAT41, none of the 5-nm clusters (marking endogenous LAT) contain 10-nm gold marking the CD4 extracellular domain of the recombinant protein (Figure 7D). As expected, analysis of wild-type chimera and endogenous LAT by using Ripley's K function shows extensive colocalization (Figure 7E). CD4-LAT41 and endogenous LAT fail to meet the Ripley's test for colocalization (Figure 7F).

Figure 5 (facing page). Spectral imaging shows osmium concentration within the dark patches of membrane. (A) Bright-field STEM image of an OsO_4-stained membrane sheet from an antigen-stimulated cell. Two electron-dense patches are apparent; one contains a 10-nm gold particle marking FcεRI β. (B) Annular dark field image of the area that includes both dark patches in A, identified by shape and the presence of the same gold particle. The graph at bottom plots the composite x-ray spectra for carbon, and oxygen and osmium over a region within the STEM image. Two distinct X-lines for osmium are plotted (Os-M and Os-L). (C) Carbon component image calculated by AXSIA from the spectral image data set. (D) Osmium component image (OsM line) calculated by AXSIA from the same region.

DISCUSSION

Membrane raft fractions isolated by detergent extraction and sucrose gradient centrifugation are typically enriched for saturated glycerophospholipids, cholesterol, gangliosides, and proteins with cotranslational or posttranslational lipid modifications. Proteins considered to be raft markers include a number of cytoplasmic signaling proteins that are fatty acylated on amide-linked myristate and/or thioester-linked palmitate, proteins anchored to the outer lipid bilayer through covalently linked glycosylphosphatidylinositols, and proteins that are isoprenylated on cysteine residues near the carboxy terminus (Brown and London, 1998, 2000). The problem we address is the relationship of raft components to their distributions in the membrane before detergent extraction and fractionation. We show that whereas two raft markers *can* mix, the extent to which they *do* mix would be difficult to predict by methods that disturb the native membrane. GPI-anchored Thy-1 and GM1 ganglioside do not mix in the mast cell membrane, in agreement with fluorescence resonance energy transfer studies of GM1 and three different GPI-anchored proteins in HeLa and normal rat kidney cells (Kenworthy *et al.*, 2000). Thy-1 and palmitoylated LAT clusters show a small amount of mixing that is markedly enhanced after Thy-1 aggregation. Thy-1 and LAT are inherently clustered, whereas GM1 is not. None of the raft markers follow cross-linked FcεRI into electron-dense regions of membrane, although aggregated GM1 can be independently recruited to these dark patches.

It should not be surprising that the different classes of lipid modification are not equivalent when determining their location in native membranes, despite their similar buoyant densities after detergent extraction and gradient centrifugation. There are important temporal and biochemical characteristics to consider. For example, myristoylation occurs cotranslationally and is essentially irreversible, whereas palmitoylation is both inducible and reversible (reviewed in Bhatnager and Gordon, 1997). Prenylated proteins often have a second membrane-targeting site, for example, the palmitoylation sites and clusters of basic amino acid residues found on different Ras species (Hancock *et al.*, 1989, 1990). Hancock's group used immunogold labeling to localize GFP molecules modified with the nine N-terminal amino acids of H-ras or the 17 N-terminal amino acid residues of K-ras on membrane sheets (Prior *et al.*, 2001). The H-ras sequence, with both palmitoylation and farnesylation sites, targeted a small fraction of the fusion protein to caveolae. The K-ras sequence, with farnesylation sites and a polybasic stretch, did not. Wild-type H-ras, but not GTP-bound forms of H-ras, were sometimes found in caveolae, suggesting that the nucleotide state of GTPases influences domain targeting. Others have used reconstitution assays to measure association of engineered G proteins with membranes that mimic the l_o phase (Moffett *et al.*, 2000). Myristoylation and palmitoylation were found to be both necessary and sufficient for partitioning into these membranes and substitution of a *cis*-unsaturated fatty acid for saturated palmitate reduced the association. Proteins modified with branched, bulky prenyl groups were excluded. Because sphingolipids have unusually long saturated acyl chains, Linder's group proposed that re-

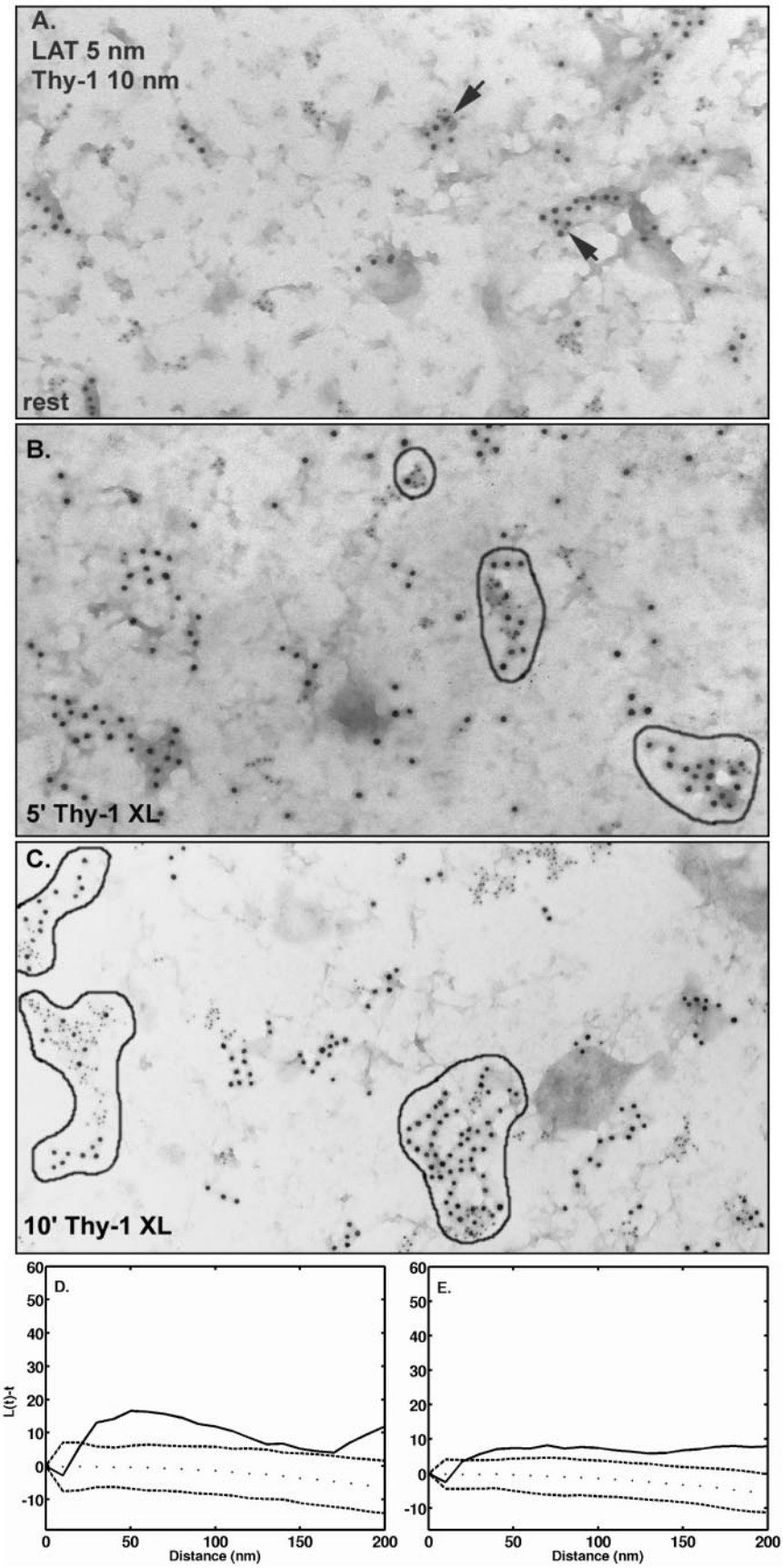

Figure 6. Coclustering of Thy-1 and LAT is increased after Thy-1 aggregation. (A) Cells were fixed with 2% paraformaldehyde and Thy-1 was labeled from the outside using anti-Thy-1-gold (10 nm). Membrane sheets were prepared and labeled from the inside with anti-LAT-gold (5 nm). Arrows mark clusters containing both sizes of gold. (B and C). Cells were incubated for 15 min at room temperature with anti-Thy-1 monoclonal antibody followed by 5 min (B) or 10 min (C) at 37°C with 10-nm antimouse-gold aggregate Thy-1. Sheets were prepared, fixed, and labeled from the inside with anti-LAT-gold (5 nm). Clusters containing both sides of gold are outlined in black. (D and E). Analysis of the distributions shown in A and C by using the Ripley's K statistic. (D and E). Experimental values for $L(t) - t$ (solid line) fall outside the boundaries predicted for pairwise sets of random points (dotted lines), confirming Thy-1 and LAT colocalization in both resting membranes and in membranes after 10 min of Thy-1 aggregation.

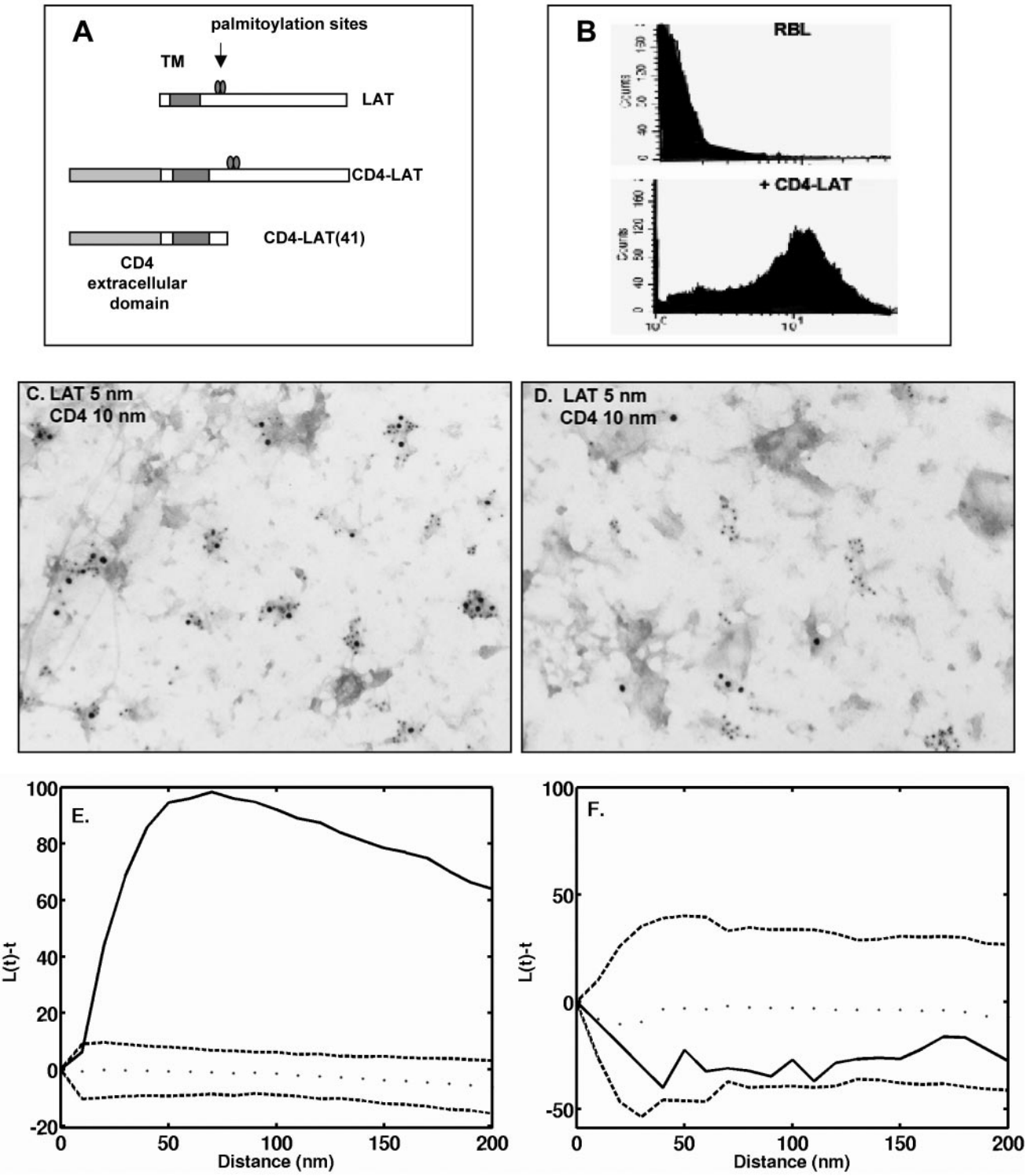

Figure 7. Chimeric CD4-LAT, but not CD4-LAT lacking the cytoplasmic tail, coclusters with endogenous LAT. (A) Schematic of CD4-LAT constructs used for stable transfection of RBL-2H3 cells. (B) Surface expression of CD4 analyzed by use of fluorescent anti-CD4 antibodies and flow cytometry. (C and D) Cells stably expressing CD4-LAT (C) or CD4-LAT 41 (D) were fixed with paraformaldehyde and then labeled from the outside with anti-CD4 gold (10 nm). Membrane sheets were prepared and labeled from the inside with anti-Lat gold (5 nm). (C) Coclustering of CD4-LAT wild type with endogenous LAT. (D) Lack of coclustering of the truncated CD4-LAT41 with endogenous LAT. (E and F). Use of Ripley's K statistic to confirm the coclustering of CD4-LAT with endogenous LAT (E) and the lack of colocalization of CD4-LAT41 with endogenous LAT (F).

cruitment into l_o domains is not simply due to the addition of a hydrophobic moiety but is dependent on the ability of saturated lipids to pack tightly (Moffett *et al.*, 2000). Proteins like H-Ras and heterotrimeric G proteins contain potentially conflicting signals, because they are both prenylated and fatty acylated. One explanation offered is the possibility that such restricted signaling proteins may have productive interactions at the edges of l_o rafts. Our work documenting the presence of signaling molecules like PLCγ1 and phosphatidylinositol 3-kinase at the border of LAT rafts (Wilson *et al.*, 2001) is consistent with Linder's prediction. We report here that the ability of chimeric CD4-LAT to cluster and incorporate into rafts of endogenous LAT is dependent on its cytoplasmic tail, which includes both palmitoylation and tyrosine phosphorylation sites; we expect that acylation is the critical factor, because LAT mutants lacking the cysteine palmitoylation sites fail to reconstitute signaling in LAT-deficient cells (Zhang *et al.*, 1998).

It is intriguing that cross-linked IgE receptors and aggregated GM1 concentrate in regions that accumulate osmium, which reacts with double bonds in unsaturated fatty acids. However, we note that osmium may also label *trans*-double bonds present in sphingomyelins. Cholesterol is another potential target of osmium, based upon oxidation of androstenolone that shares the same 5,6 double bond as cholesterol (Batan, 1960). Along with actively signaling receptors, these regions recruit a long list of signaling proteins, including tyrosine kinases (Syk and BTK), adaptors and guanine nucleotide exchange factors (Gab2, Grb2, and Vav), enzymes involved in phosphoinositide metabolism (PLCγ2, PI 3-kinase, and PTEN), and negative regulatory molecules (Cbl) (Wilson *et al.*, 2001, 2002). Antigen-bound receptors in immunoreceptor "signalosomes" (Fruman *et al.*, 2000) are likely to be stabilized by physical cross-links. If receptors are surrounded by less ordered unsaturated lipids, it is possible that other constituents of the signalosomes are highly mobile. Live cell imaging experiments are in progress to test this hypothesis.

We show that coated pits bud from the periphery of osmiophilic patches. Cross-linked FcεRI and GM1 are selectively internalized through these pits. In contrast, label for Thy-1 is neither concentrated in nor excluded from the patches or their neighboring coated pits, suggesting a relative absence of topographical constraints for this GPI-linked protein even after external cross-linking. It is known that clathrin-coated pits bud from topographically restricted membrane regions, including the uropods of polarized macrophages and neutrophils and the cleavage furrows of dividing cells (Pfeiffer *et al.*, 1980; Oliver and Berlin, 1983) and that multiple vesicles may form from a single pit (Gaidarov *et al.*, 1999; illustrated in Wilson *et al.*, 2000). This, and other recent work (Blanpied *et al.*, 2002), suggests cells can organize "hot spots" that are sites of repeated rounds of clathrin vesicle formation. The osmiophilic membrane patches observed here may represent these sites.

We conclude that the topographical relationships between membrane proteins and lipids are not adequately revealed by methods that disturb the native membrane. Lipid raft analysis by detergent extraction and membrane fractionation cannot distinguish between different rafts with similar buoyancy but unique and dynamic compositions. Lipid rafts are estimated by several groups to be <70 nm in diameter (Friedrichson and Kurzhalia, 1998; Varma and Mayor, 1998; Pralle *et al.*, 2000), which is below the resolution (>200 nm) of light microscopy. Thus, standard epifluorescence microscopy has been of limited use to study membrane raft heterogeneity except when raft components are physically polarized by cell–cell interaction or orientation in a chemotactic gradient. Examples include evidence that LAT associates only transiently, and a YFP-GPI construct not at all, with TCR rafts formed by coating coverslips with stimulatory antibodies and imaging at the point of tight contact between T cell and coverslip (Bunnell *et al.*, 2002) and other evidence that polarized migrating T cells distribute different raft markers to the leading edge and the uropod (Millan *et al.*, 2002). The application of fluorescence resonance energy transfer dramatically improves the ability to measure pairs of interacting molecules at 50-angstrom resolution and in real time but domain size is not measured. By electron microscopic examination of gold-labeled membrane sheets from resting cells, we show here that clusters of FcεRI and Thy-1 are indeed very small (20–50 nm) and that GM1 is rarely clustered at all. When cross-linked externally, all three membrane components redistribute independently to membrane domains that can exceed 500 nm in diameter. In contrast, aggregation of Thy-1 promotes the colocalization of Thy-1 and LAT microdomains. These domains are likely to be stabilized by a combination of physical cross-links and the merging of lipid shells theorized to surround individual components (Anderson and Jacobson, 2002). Reinforcing the heterogeneity of membrane organization, it is remarkable that each of these membrane components exhibits independent behavior, with GM1 showing an inherently random distribution but becoming topographically restricted after cross-linking and Thy-1 distributing as clusters whose topography seemed to be unconstrained even after external cross-linking. Thus, electron microscopy reveals a much more complex and dynamic topographical organization of membrane domains than is predicted by biochemical analysis of detergent-resistant membranes or observed to date by fluorescence microscopy.

ACKNOWLEDGMENTS

This work is a memorial to Dr. Carla Wofsy, a pioneer in the spatial analysis of FcεRI distribution and in mathematical modeling of early events in receptor signaling. The project was supported by National Institutes of Health grants R01 AI051575, R01 GM49814, and P20 GM66283 and by New Mexico Tobacco Settlement funds awarded to the University of New Mexico Cancer Research and Treatment Center. J.Z. is a graduate fellow of the Gies Foundation, University of New Mexico Cancer Research and Treatment Center. Sandia is a multiprogram laboratory operated by Sandia Corporation, A Lockheed Martin Company, for the United States Department of Energy under contract DC-AC04-94AL85000. Use of the electron microscopy facilities at the University of New Mexico Health Sciences Center and Sandia National Laboratory is gratefully acknowledged. We thank Robert Murphy (National Jewish Medical and Research Center) for insightful discussion.

REFERENCES

Ahmed, S.N., Brown, D.A., and London, E. (1997). On the origin of sphingolipid/cholesterol-rich detergent-insoluble cell membranes: physiological concentrations of cholesterol and sphingolipid induce formation of a detergent-insoluble, liquid-ordered lipid phase in model membranes. Biochemistry *36*, 10944–10953.

Anderson, R.G.W. (1998). The caveolae membrane system. Annu. Rev. Biochem. *67*, 199–225.

Anderson, R.G.W., and Jacobson, K. (2002). A role for lipid shells in targeting proteins to caveolae, rafts and other lipid domains. Science *296*, 1821–1825.

Batan, J.S. (1960). Method for the cleavage of osmate esters. J. Organic Chem. *25*, 257.

Bhatnager, R.S., and Gordon, J.I. (1997). Understanding covalent modifications of proteins by lipids: where cell biology and biophysics mingle. Trends Cell Biol. *7*, 14–20.

Blanpied, T.A., Scott, D., and Ehlers, M.D. (2002). Dynamics and regulation of clathrin coats at specialized endocytic zones of dendrites and spines. Neuron *36*, 435–449.

Brown, D.A., and London, E. (1998). Functions of lipid rafts in biological membranes. Annu. Rev. Cell Dev. Biol. *14*, 111–136.

Brown, D.A., and London, E. (2000). Structure and function of sphingolipid- and cholesterol-rich membrane rafts. J. Biol. Chem. *275*, 17221–17224.

Bunnell, S.C., Hong, D.L., Kardon, J.R., Yamazaki, T., McGlade, C.J., Barr, V.A., and Samelson, L.E. (2002). T cell receptor ligation induces the formation of dynamically regulated signaling assemblies. J. Cell Biol. *158*, 1263–1275.

Draberova, L., and Draber, P. (1993). Thy-1 glycoprotein and src-like protein-tyrosine kinase p53/p56(lyn) are associated in large detergent-resistant complexes in rat basophilic leukemia-cells. Proc. Natl. Acad. Sci. USA *90*, 3611–3615.

Draber, P., and Draberova, L. (2002). Lipid rafts in mast cell signaling. Mol. Immunol. *38*, 1247–1252.

Edidin, M. (1997). Lipid microdomains in cell surface membranes. Curr. Opin. Struct. Biol. *7*, 528–532.

Edidin, M. (2001). Shrinking patches and slippery rafts: scales of domains in the plasma membrane. Trends Cell Biol. *11*, 492–496.

Field, K.A., Holowka, D., and Baird, B. (1995). FcεRI-mediated recruitment of p53/56(lyn) to detergent-resistant membrane domains accompanies cellular signaling field. Proc. Natl. Acad. Sci. USA *92*, 9201–9205.

Field, K.A., Holowka, D., and Baird, B. (1997). Compartmentalized activation of the high affinity immunoglobulin E receptor within membrane domains. J. Biol. Chem. *272*, 4276–4280.

Field, K.A., Holowka, D., and Baird, B. (1999). Structural aspects of the association of FcεRI with detergent-resistant membranes. J. Biol. Chem. *274*, 1753–1758.

Friedrichson, T., and Kurzhalia, T. (1998). Microdomains of GPI-anchored proteins in living cells revealed by chemical crosslinking. Nature *394*, 802–805.

Fruman, D.A., Satterthwaite, A.B., and Witte, O.N. (2000). Xid-like phenotypes: a B cell signalosome takes shape. Immunity *13*, 1–3.

Gaidarov, I., Santini, F., Warren, R.A., and Keen, J.H. (1999). Spatial control of coated-pit dynamics in living cells. Nat. Cell Biol. *1*, 1–7.

Haase, P. (1995). Spatial pattern analysis in ecology based on Ripley's K-function: introduction and methods of edge correction. J. Vegetation Sci. *6*, 575–582.

Hancock, J.F., Cadwallader, K., Paterson, H., and Marchal, C.J. (1989). All ras proteins are polyisoprenylated but only some are palmitoylated. Cell *57*, 1167–1177.

Hancock, J.F., Paterson, H., and Marchal, C.J. (1990). A polybasic domain or palmitoylation is required in addition to the CAAX motif to localize p21 ras to the plasma membrane. Cell *63*, 133–139.

Harder, T., and Kuhn, M. (2000). Selective accumulation of raft-associated membrane protein LAT in T cell receptor signaling assemblies. J. Cell Biol. *151*, 199–207.

Ilangumaran, S., Arni, S., vanEchtenDeckert, G., Borisch, B., and Hoessli, D.C. (1999). Microdomain-dependent regulation of Lck and Fyn protein-tyrosine kinases in T lymphocyte plasma membranes. Mol. Biol. Cell. *10*, 891–905.

Jacobson, K., and Dietrich, C. (1999). Looking at lipid rafts? Trends Cell Biol. *9*, 87–91.

Jain, A.J., and Dubes, R.C. (1988). Algorithms for Clustering, Englewood Cliffs, NJ, Prentice Hall.

Kenworthy, A.K., Petranova, N., and Edidin, M. (2000). High-resolution FRET microscopy of cholera toxin B-subunit and GPI-anchored proteins in cell plasma membranes. Mol. Biol. Cell *11*, 1645–1655.

Kotula, P.G., Keenan, M.R., and Michael, J.R. (2003). Automated analysis of SEM X-Ray spectral images: a powerful new microanalysis tool. Microsc. Microanal. *9*, 1–17.

Langlet, C., Bernard, A.-M., Drevot, P., and He, H.-T. (2000). Membrane rafts and signaling by the multichain immune recognition receptor. Curr. Opin. Immunol. *12*, 250–255.

March, J. (1977). Addition to carbon-carbon multiple bonds. In: Advanced Organic Chemistry: Reactions, Mechanisms, and Structure, 2nd ed., New York: McGraw-Hill Book Company, 748–749.

Mayor, S., and Maxfield, F.R. (1995). Insolubility and redistribution of GPI-anchored proteins at the cell surface after detergent treatment. Mol. Biol. Cell *6*, 929–944.

Millan, J., Montoya, M.C., Sancho, D., Sanchez-Madrid, F., and Alonso, M.A. (2002). Lipid rafts mediate biosynthetic transport to the T lymphocyte uropod subdomain and are necessary for uropod integrity and function. Blood *99*, 978–984.

Moffett, S., Brown, D.A., and Linder, M.E. (2000). Lipid-dependent targeting of G proteins into rafts. J. Biol. Chem. *275*, 2191–2198.

Montixi, C., Langlet, C., Bernard, A.M., Thimonier, J., Dubois, C., Wurbel, M.A., Chauvin, J.P., Pierres, M., and He, H.T. (1998). Engagement of T cell receptor triggers its recruitment to low-density detergent-insoluble membrane domains. EMBO J. *17*, 5334–5348.

Oliver, J.M., and Berlin, R.D. (1983). Surface and cytoskeleton events regulating leukocyte membrane topography. Sem. Hematol. *20*, 282–304.

Parolini, I., Topa, S., Sorice, M., Pace, A., Ceddia, A., Montesoro, E., Pavan, A., Linasanti, M.P., Peschle, C., and Sargiacomo, M. (1999). Phorbol ester-induced disruption of the CD4-Lck complex occurs within a detergent-resistant microdomain of the plasma membrane - Involvement of the translocation of activated protein kinase C isoforms. J. Biol. Chem. *274*, 14176–14187.

Pfeiffer, J.R., Oliver, J.M., and Berlin, R.D. (1980). Topographical distribution of coated pits. Nature *286*, 727–728.

Philimonenko, A.A., Janacek, J., and Hozak, P. (2000). Statistical evaluation of colocalization patterns in immunogold labeling experiments. J. Struct. Biol. *132*, 201–210.

Pralle, A., Keller, P., Florin, E.-L., Simons, K., and Hörber, J.K.H. (2000). Sphingolipid–cholesterol rafts diffuse as small entities in the plasma membrane of mammalian cells. J. Cell Biol. *148*, 997–1008.

Prior, A.I., Harding, A., Yan, J., Sluimer, J., Parton, R.G., and Hancock, J.F. (2001). GTP-dependent segregation of H-ras from lipid rafts is required for biological activity. Nat. Cell Biol. *3*, 368–375.

Prior, I.A., Muncke, C., Parton, R.G., and Hancock, J.F. (2003). Direct visualization of Ras proteins in spatially distinct cell surface microdomains. J. Cell Biol. *160*, 165–170.

Reed, R.A., Mattai, J., and Shipley, G.G. (1987). Interaction of cholera-toxin with ganglioside GM1 receptors in supported lipid monolayers. Biochemistry *26*, 824–832.

Ribi, H.O., Ludwig, D.S., Mercer, K.L., Schoolnik, G.K., and Kornberg, R.D. (1988). Dimensional structure of cholera-toxin penetrating a lipid-membrane. Science *239*, 1272–1276.

Saitoh, S., Arudchandran, R., Manetz, T.S., Zhang, W.G., Sommers, C.L., Love, P.E., Rivera, J., and Samelson, L.E. (2000). LAT is essential for FcεRI-mediated mast cell activation. Immunity *12*, 525–535.

Schroeder, R., London, E., and Brown, D. (1994). Interactions between saturated acyl chains confer detergent resistance on lipids and glycosylphosphatidylinositol (GPI)-anchored proteins: GPI-anchored proteins in liposomes and cells show similar behavior. Proc. Natl. Acad. Sci. USA *91*, 12130–12134.

Simons, K., and Ikonen, E. (1997). Functional rafts in cell membranes. Nature *387*, 569–572.

Stauffer, T.P., and Meyer, T. (1997). Compartmentalized IgE receptor-mediated signal transduction in living cells. J. Cell Biol. *139*, 1447–1454.

Surviladze, Z., Dráberová, L., Kovárová, L., Boubelik, M., and Dráber, P. (2001). Differential sensitivity to acute cholesterol lowering of activation mediated via the high-affinity IgE receptor and Thy-1 glycoprotein. Eur. J. Immunol. *31*, 1–10.

Surviladze, Z., L. Dráberová, L. Kubinová, and P. Dráber, P. (1998). Functional heterogeneity of Thy-1 membrane microdomains in rat basophilic leukemia cells. Eur. J. Immunol. *28*, 1847–1858.

Varma, R., and Mayor, S. (1998). GPI-anchored proteins are organized in submicron domains at the cell surface. Nature *394*, 798–801.

Wilson, B.S., Kapp, N., Lee, R.J., Pfeiffer, J.R., Martinez, A.M., Platt, Y., Letourneur, F., and Oliver, J.M. (1995). Distinct functions of the FcεRI β and γ subunits in the control of FcεRI-mediated tyrosine kinase activation and signaling responses in RBL-2H3 mast cells. J. Biol. Chem. *270*, 4013–4022.

Wilson, B.S., Pfeiffer, J.R., and Oliver, J.M. (2000). Observing FcεRI signaling from the inside of the mast cell membrane. J. Cell Biol. *149*, 1131–1142.

Wilson, B.S., Pfeiffer, J.R., Surviladze, Z., Gaudet, E.A., and Oliver, J.M. (2001). High resolution mapping reveals distinct FcεRI and LAT domains in activated mast cells. J. Cell Biol. *154*, 645–658.

Wilson, B.S., J. R. Pfeiffer and J. M. Oliver, J.M. (2002). FcεRI signaling observed from the inside of the mast cell membrane. Mol. Immunol. *38*, 1259–1268.

Wofsy, C., Sanders, M.L., Donahoe, G.W., Pujol, M., and Oliver, J.M. (1995). Quantifying IgE receptor aggregation from SEM-immunocytology. Microsc. Microanal. *1*, 782–784.

Zhang, W.G., Trible, R.P., and Samelson, L.E. (1998). LAT palmitoylation: its essential role in membrane microdomain targeting and tyrosine phosphorylation during T cell activation. Immunity *9*, 239–246.